



**Politecnico
di Torino**

Politecnico di Torino

Master of Science in Energy and Nuclear Engineering

01FJIXY - Computational Thermomechanics

A.Y. 2025/2026

HOMEWORK 08 - PLATE WITH HOLE IN PLASTICITY

Tommaso COGOZZO

1 Problem statement and given data

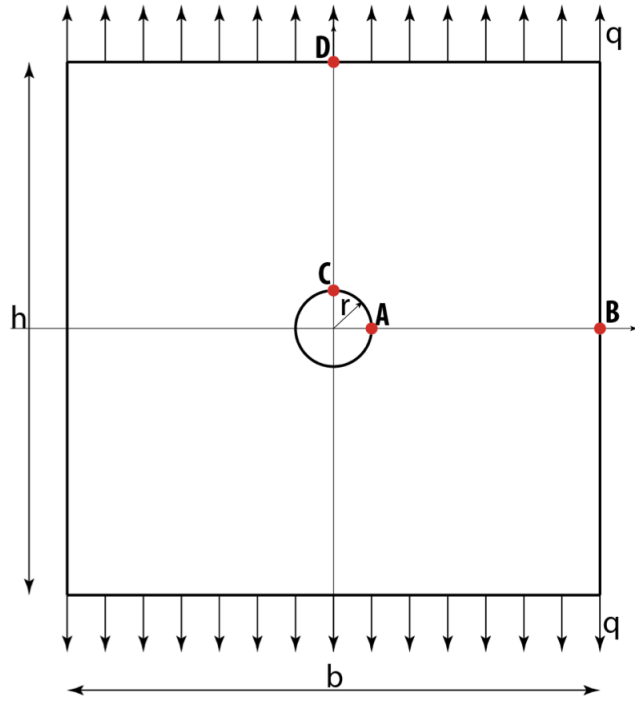


Figure 1: Plate with circular hole and a uniform load applied on the top and bottom side

Data:

- Width: $b = 0.7 \text{ m}$
- Height: $h = 0.7 \text{ m}$
- Thickness: $t = 0.01 \text{ m}$
- Hole radius: $R = 0.05 \text{ m}$
- Elasticity modulus: $E = 2.1 \times 10^{11} \text{ N/m}^2$
- Poisson's ratio: $\nu = 0.3$
- Applied load: $q = 2.0 \times 10^6 \text{ N/m}$
- Yield stress: $\sigma_p = 2.4 \times 10^8 \text{ N/m}$
- Applied displacement: $v = 0.4 \text{ mm}$

2 Objective

The problem of a rectangular plate with a central circular hole subjected to a uniformly distributed load applied on the upper and lower edges can be analytically addressed by means of the classical *Kirsch solution*. Under the assumption of linear elastic behavior and an infinite plate, the stress field induced by a circular hole of radius r subjected to a uniform remote stress σ_∞ can be expressed in polar coordinates (ρ, θ) , with the origin located at the center of the hole.

In the present case, the nominal remote stress is defined as

$$\sigma_\infty = \frac{q}{t}, \quad (1)$$

where q denotes the uniformly distributed load per unit length applied on the plate edges and t is the plate thickness.

According to Kirsch's analytical solution, the stress components in polar coordinates are given by:

$$\sigma_{rr} = \frac{\sigma_\infty}{2} \left(1 - \frac{r^2}{\rho^2} \right) + \frac{\sigma_\infty}{2} \left(1 - 4 \frac{r^2}{\rho^2} + 3 \frac{r^4}{\rho^4} \right) \cos(2\theta), \quad (2)$$

$$\sigma_{\theta\theta} = \frac{\sigma_\infty}{2} \left(1 + \frac{r^2}{\rho^2} \right) - \frac{\sigma_\infty}{2} \left(1 + 3 \frac{r^4}{\rho^4} \right) \cos(2\theta), \quad (3)$$

$$\tau_{r\theta} = -\frac{\sigma_\infty}{2} \left(1 + 2 \frac{r^2}{\rho^2} - 3 \frac{r^4}{\rho^4} \right) \sin(2\theta). \quad (4)$$

These relations are valid only within the linear elastic regime. However, since the present problem is investigated in the *elastoplastic* range, the Kirsch solution ceases to be applicable once the stress state exceeds the material yield stress σ_p . Consequently, the analytical expressions reported above can be considered valid only up to the onset of yielding.

Figure 2 illustrates the distribution of the circumferential stress $\sigma_{\theta\theta}$ along the horizontal symmetry axis **AB**, as predicted by the elastic Kirsch solution. This stress distribution is physically meaningful only until the yielding limit is reached. Beyond this threshold, plastic effects dominate the mechanical response of the structure, and the stress field can no longer be described analytically. Therefore, the post-yield behavior must be evaluated exclusively through numerical methods.

The main objective of this report is to investigate the mechanical behavior of a rectangular plate with a central circular hole subjected to uniform loading applied on the upper and lower boundaries, considering an elastoplastic material model. The analysis is carried out by comparing the analytical elastic solution provided by Kirsch with the numerical results obtained using the finite element code **FEAP**, with the following specific objectives:

- to evaluate the stress distribution along the symmetry axes **AB** (horizontal axis) and **CD** (vertical axis);

- to analyze the evolution of stresses at the characteristic points **A**, **B**, and **C**;
- to observe the initiation and propagation of the plastic zone as the applied load is progressively increased;
- to assess the influence of mesh refinement on the accuracy and convergence of the numerical results.

In order to reduce the computational cost, the double symmetry of both geometry and loading conditions has been exploited. As a result, only one quarter of the plate has been modeled, enforcing appropriate symmetry boundary conditions along the corresponding axes, without compromising the accuracy of the numerical solution.

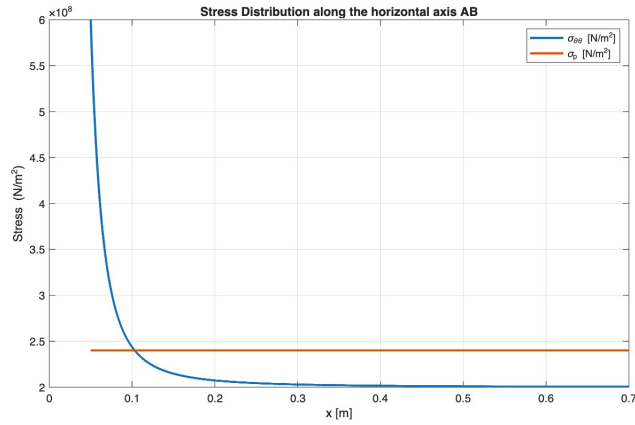


Figure 2: Analytical stress distribution along AB (elastic problem)

3 Finite Element Analysis with 3-Nodes Triangular Elements

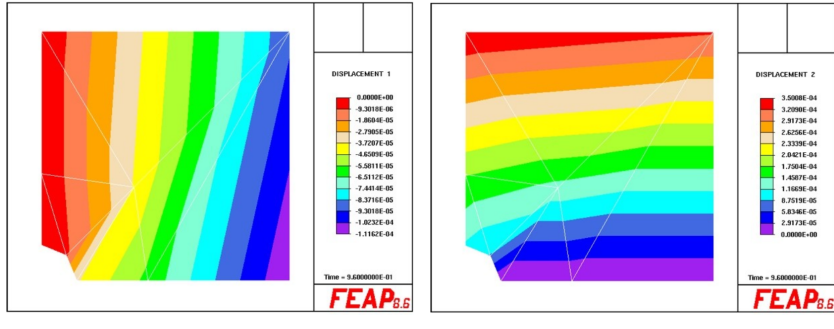


Figure 3: Computed displacement distributions $mr = 1$

First, Figure 3 presents the numerical distributions of the horizontal and vertical displacement components. Since only a portion of the computational domain was modeled in order to exploit geometric symmetry, appropriate boundary constraints were imposed along the two Cartesian axes.

The obtained results show, as expected, zero displacement values in proximity to the constrained boundaries. This behavior confirms the correct implementation of the symmetry boundary conditions and validates the interface treatment associated with the adopted subdomain.

A series of mesh discretizations using triangular elements was implemented in order to assess the capability of the numerical model to accurately reproduce the expected stress distributions. Figure 4 reports the colormaps corresponding to the stress distributions in their horizontal and vertical components (Figures 4a and 4b, respectively) computed with mesh refinement equal to 1.

The analysis conducted at time $t = 0.96$ s shows the distribution of the equivalent Von Mises stress (σ_{vM}) over the analyzed geometry. This parameter was adopted as the failure criterion to evaluate the structural integrity of the component under complex loading conditions. The Von Mises equivalent stress is defined as:

$$\sigma_{\text{vM}} = \sqrt{\frac{1}{2} [(\sigma_x - \sigma_y)^2 + (\sigma_y - \sigma_z)^2 + (\sigma_z - \sigma_x)^2] + 3 (\tau_{xy}^2 + \tau_{yz}^2 + \tau_{zx}^2)} \quad (5)$$

where σ_x , σ_y , and σ_z are the normal stress components, and τ_{xy} , τ_{yz} , and τ_{zx} are the shear stress components.

The maximum equivalent stress obtained from the simulation is:

$$\sigma_{vM,\max} \approx 2.19 \times 10^8 \text{ N/m}^2 \quad (219.4 \text{ MPa}) \quad (6)$$

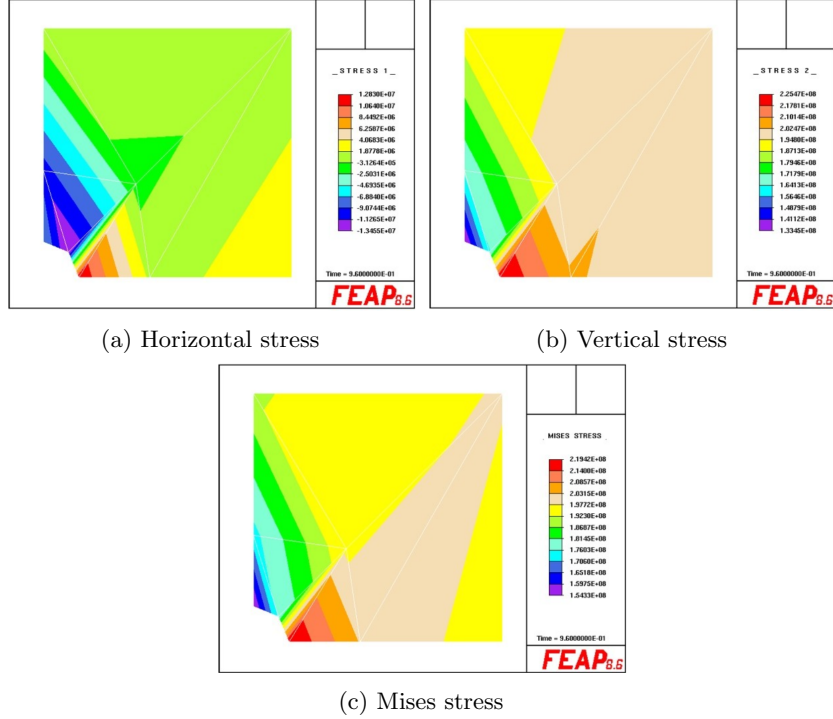


Figure 4: Computed stress distributions $m_r = 1$

Comparing this value with the material yield strength provided, $\sigma_p = 2.4 \times 10^8 \text{ N/m}^2$, it can be observed that:

$$\sigma_{vM,\max} < \sigma_p \quad (7)$$

Since the maximum Von Mises stress is lower than the yield stress, the material remains entirely within the elastic regime. Therefore, at the considered time instant, no permanent plastic deformations occur.

To complete the analysis of the stress state of the component, the stress profiles computed along selected directions (segments CD and AB) are reported for different values of the parameter m_r ($m_r = 1, 5, 50$). These plots allow the evaluation of the influence of the stiffness- or mesh-related parameter on the local stress distribution.

The first graph illustrates the horizontal stress distribution (N/m^2) as a function of the coordinate y . A strongly nonlinear behavior is observed in the initial portion of the domain ($y < 0.10 \text{ m}$).

Gradient effect: For higher values of m_r (5 and 50), a pronounced concentration of compressive stresses (negative values) is detected, reaching peaks close to $-2.5 \times 10^8 \text{ N/m}^2$. Conversely, the case $m_r = 1$ exhibits an almost flat profile, suggesting that the parameter m_r plays a crucial role in capturing stress

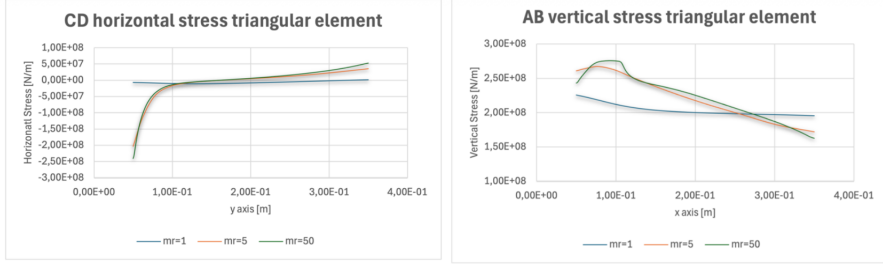


Figure 5: Stress distribution on CD and AB

singularities or steep gradients near constraints or boundaries.

Convergence behavior: Beyond $y = 0.15$ m, all profiles progressively stabilize toward values close to zero, indicating that the horizontal stress in that region becomes negligible or that the local perturbation effects decay with distance from the constrained area.

The second graph presents the vertical stress distribution (N/m^2) along the x -axis. This diagram is particularly significant, as the reported values intersect or exceed the previously defined yield strength ($\sigma_p = 2.4 \times 10^8 \text{ N}/\text{m}^2$).

Exceedance of the yield stress: For $m_r = 5$ and $m_r = 50$, the vertical stress exhibits a peak exceeding $2.5 \times 10^8 \text{ N}/\text{m}^2$ within the region $0.05 \text{ m} \leq x \leq 0.12 \text{ m}$. This indicates that, according to these models, local plasticization is initiated in this area, since

$$\sigma_{\text{vertical}} > \sigma_p.$$

Dependence on m_r : Once again, the model with $m_r = 1$ significantly underestimates the stress peak, remaining consistently below the safety threshold. This highlights the importance of an appropriate selection of the parameter m_r (likely related to mesh refinement or to a material stiffness ratio) for a conservative and reliable structural strength assessment.

Asymptotic trend: For $x > 0.20$ m, the vertical stress gradually decreases for all configurations, stabilizing within a safe range between 1.5×10^8 and $2.0 \times 10^8 \text{ N}/\text{m}^2$.

The comparison between the two diagrams clearly indicates that the vertical stress along segment AB represents the most critical loading condition for the structural integrity of the component. While the horizontal stress remains confined or predominantly compressive, the vertical stress exceeds the elastic capacity of the material for configurations with $m_r \geq 5$. From a design perspective, this evidence suggests the need for either a geometric modification or the selection of a material with a higher yield strength in order to prevent permanent deformations in the regions identified by the stress peaks.

The spatial distributions (colormaps) of the Von Mises equivalent stress and of the horizontal and vertical stress components are presented here for the highest-resolution configuration ($m_r = 50$).

Such a multiaxial analysis is required to discriminate the contribution of the

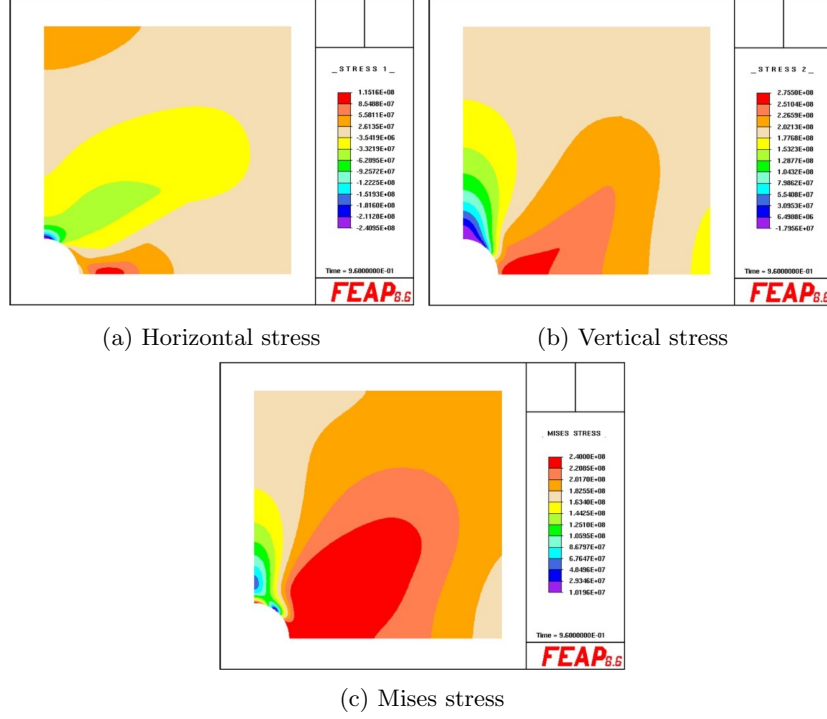


Figure 6: Computed stress distributions $mr = 50$

individual stress components to the overall mechanical state of the material. While the directional stress maps enable identification of the nature of the loading condition (tension or compression) along the principal axes, the Von Mises map synthesizes these combined effects into a single scalar indicator.

This representation facilitates a direct comparison with the material yield strength, equal to $2.4 \times 10^8 \text{ N/m}^2$, thereby confirming the elastic stability of the component under the considered loading conditions.

4 Finite Element Analysis with 4-Nodes Rectangular Elements

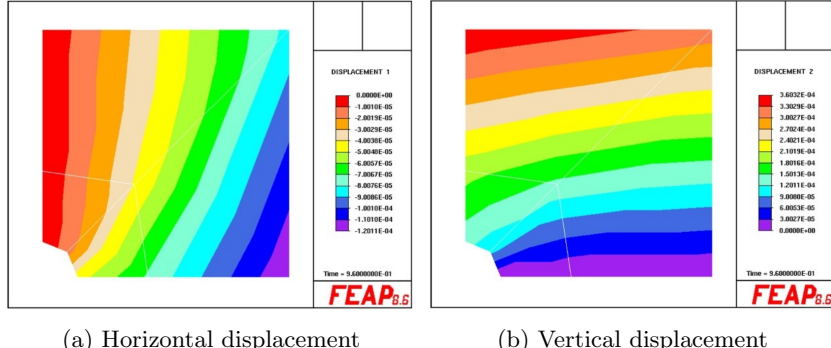


Figure 7: Computed displacement distributions $mr = 1$

The same analysis is repeated using four-node quadrilateral (rectangular) finite elements. As discussed in Section 3, the displacement distributions are reported to verify the consistency of the numerical formulation.

The results once again confirm the correct implementation of the symmetry boundary conditions: the horizontal displacement component exhibits zero values along the y -axis, while the vertical displacement component vanishes along the x -axis. This behavior is fully consistent with the imposed kinematic constraints and validates the symmetry-based reduction of the computational domain.

The corresponding results (evaluated with mesh = 1) are summarized in the colormaps shown in Figure 8. The comparison among the horizontal stress distribution (a), the vertical stress distribution (b), and the Von Mises equivalent stress (c) highlights a smoother load distribution and an improved resolution of stress gradients in the vicinity of the notch.

Despite the adoption of this different element formulation, the stress peaks remain consistent with the previous analyses, confirming the robustness of the numerical results. The critical region is still localized in the lower-left corner of the domain, where the vertical stress component is confirmed to be the dominant contribution to the Von Mises equivalent stress.

As observed, rectangular elements provide a more accurate approximation of the reference solution, even when relatively coarse meshes are employed. This improved performance is particularly evident in the vicinity of the hole, where the stress field is characterized by steep gradients induced by geometric discontinuities.

In this region, the stress does not decay as rapidly as predicted by less suitable discretizations, owing to the localized deformation effects. The quadrilateral elements therefore capture more effectively the stress concentration and

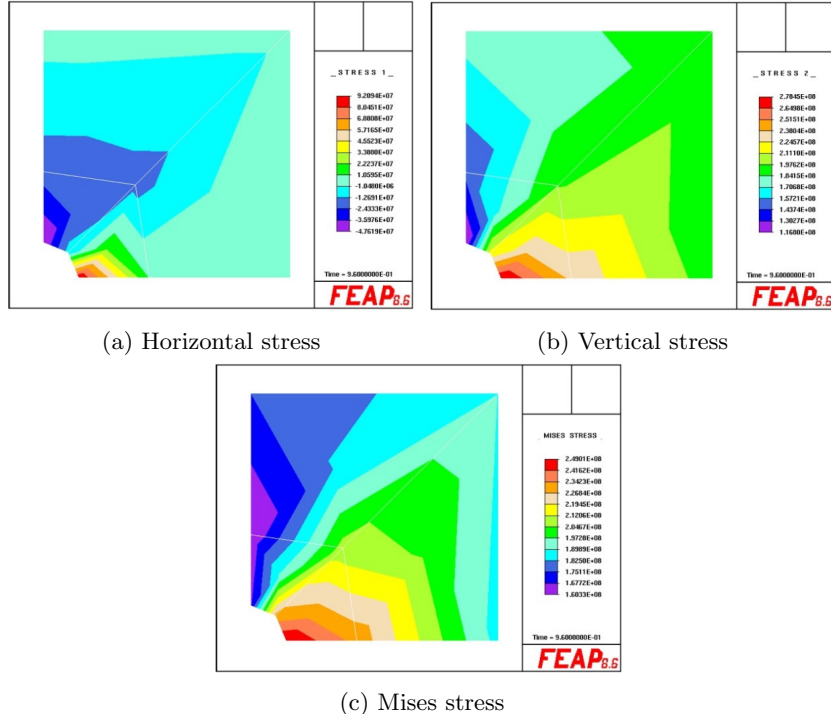


Figure 8: Computed stress distributions $mr = 1$

its spatial evolution.

At this stage of the analysis, the horizontal and vertical stress profiles extracted along segments CD and AB are examined using a discretization based on four-node quadrilateral elements. This approach allows the assessment of the model sensitivity to both the type of finite element employed and the mesh density.

The horizontal stress profile exhibits a pronounced compressive behavior near the origin, with a negative peak of approximately $-2.5 \times 10^8 \text{ N/m}^2$ for the finer meshes ($m_r = 5, 50$). Compared to triangular elements, a smoother gradient distribution and a clearer convergence between the cases $m_r = 5$ and $m_r = 50$ can be observed. This indicates that quadrilateral elements provide superior accuracy in regions subjected to strong lateral compression.

The vertical stress distribution along segment AB proves to be critical. For $m_r = 50$, the stress peak reaches approximately $2.75 \times 10^8 \text{ N/m}^2$. This result is of particular importance for two main reasons:

Comparison with the yield strength: Unlike the previous analyses, the maximum value obtained using quadrilateral elements clearly exceeds the yield threshold, $\sigma_p = 2.4 \times 10^8 \text{ N/m}^2$. This finding indicates that the use of a more accurate element formulation enables the detection of local plasticization that

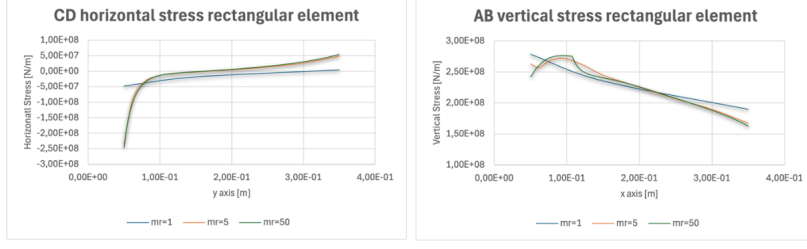


Figure 9: Stress distribution on CD and AB

the simplified triangular model was not able to fully capture.

Comparison with triangular elements: Quadrilateral elements exhibit lower numerical stiffness and are therefore capable of reproducing higher stress peaks (approximately 20% greater than those predicted by the triangular model). This suggests that the triangular discretization was affected by a numerical stiffening effect, leading to an underestimation of the actual stress level.

In conclusion, the adoption of quadrilateral elements in the analysis corresponding to Figure 9 results in a more conservative and realistic assessment of structural safety. While the Von Mises colormaps provide a global indication of the stress state, the pointwise analysis along segment AB reveals that, in the region characterized by the maximum stress gradient, the material locally exceeds the elastic limit. Consequently, a revision of the geometry or the selection of a material with a higher yield strength is required to ensure the structural integrity of the component.

5 Conclusions

The mechanical behavior of a rectangular plate with a central circular hole subjected to uniform loading has been investigated through both analytical and numerical approaches. The classical Kirsch solution provided a useful reference for the purely elastic regime, allowing a preliminary assessment of the stress concentration effects induced by the geometric discontinuity. However, as expected, the analytical solution is no longer applicable once the stress state approaches or exceeds the material yield strength, thus requiring a numerical elastoplastic formulation.

The finite element analyses carried out with *FEAP* have highlighted the strong influence of mesh refinement and element type on the predicted stress field, particularly in the vicinity of the hole, where steep stress gradients arise. The exploitation of geometric and loading symmetries proved effective in reducing the computational cost without compromising the accuracy of the solution, as confirmed by the correct displacement constraints along the symmetry axes.

The simulations performed with 3-node triangular elements showed a clear sensitivity to the refinement parameter m_r . Coarse meshes ($m_r = 1$) significantly underestimated the peak stresses, while finer discretizations ($m_r = 5, 50$) captured higher stress concentrations along the critical segment AB. Nevertheless, a comparison with the quadrilateral formulation revealed that triangular elements tend to exhibit a certain degree of numerical stiffening, leading to a non-conservative prediction of the maximum stress.

The analyses performed with 4-node quadrilateral elements provided a smoother stress distribution and a more accurate representation of the stress gradients near the hole. In particular, for the most refined mesh ($m_r = 50$), the vertical stress peak along segment AB reached approximately $2.75 \times 10^8 \text{ N/m}^2$, clearly exceeding the material yield strength $\sigma_p = 2.4 \times 10^8 \text{ N/m}^2$. This result indicates the onset of local plasticization in the region characterized by maximum stress concentration, a phenomenon that was only partially captured by the triangular discretization.

Overall, the study demonstrates that the vertical stress component along the horizontal symmetry axis represents the most critical condition for structural integrity. The Von Mises equivalent stress maps provide a global overview of the mechanical response, while the detailed stress profiles along selected segments are essential to identify localized exceedance of the elastic limit.

From a design perspective, the results suggest that the current configuration may not guarantee full elastic behavior under the prescribed loading conditions when accurately modeled. Therefore, possible corrective measures include geometric modifications to reduce stress concentration effects or the adoption of a material with a higher yield strength. The comparison between different finite element formulations further emphasizes the importance of appropriate mesh refinement and element selection in order to obtain reliable and conservative structural assessments.